atoms

MDPI

Article

Multi-Reflection Time-of-Flight Mass Spectroscopy for Superheavy Nuclides

Peter Schury [1,*,†], Yuta Ito [2,†], Toshitaka Niwase [1,3,†] and Michiharu Wada [1,†]

[1] Wako Nuclear Science Center, Institute of Particle and Nuclear Studies, High Energy Accelerator Research Organization (KEK), Wako 351-0198, Saitama, Japan; niwase@phys.kyushu-u.ac.jp (T.N.); michiharu.wada@kek.jp (M.W.)
[2] Advanced Science Research Center, Japan Atomic Energy Agency, Tokai 319-1195, Ibaraki, Japan; ito.yuta@jaea.go.jp
[3] Department of Physics, Kyushu University, Nishi-ku 819-0395, Fukuoka, Japan
* Correspondence: schury@post.kek.jp
† These authors contributed equally to this work.

Abstract: The atomic masses of isotopes of elements beyond fermium, which can presently only be produced online via fusion-evaporation reactions, have until recently been determined only from α decay chains reaching nuclides with known atomic masses. Especially in the case of lower-yield nuclides, for which the sufficiently detailed nuclear spectroscopy required to fully determine the nuclear structure is not possible, such indirect mass determinations may suffer systematic errors. For many superheavy nuclides, their decay chains end in spontaneous fission or in β-decay prior to reaching nuclides of known mass. To address this dearth of accurate atomic masses, we have developed a multi-reflection time-of-flight mass spectrograph that can make use of decay-correlations to accurately and precisely determine atomic masses for the very low-yield superheavy nuclides.

Keywords: atomic masses; superheavy elements; MTROF

check for updates

Citation: Schury, P.; Ito, Y.; Niwase, T.; Wada, M. Multi-Reflection Time-of-Flight Mass Spectroscopy for Superheavy Nuclides. *Atoms* **2023**, *11*, 134. https://doi.org/10.3390/atoms11100134

Academic Editor: Maxime Brodeur

Received: 24 August 2023
Revised: 10 October 2023
Accepted: 14 October 2023
Published: 17 October 2023

1. Introduction

The atomic mass is one of the fundamental characteristics of atomic nuclei. The binding energy holding the nucleus together can be directly inferred from the atomic mass, making it a key probe of nuclear structures such as shell closures ("magicity") and changes in nuclear deformation. It can be argued that the effects of such nuclear structure features are of utmost importance among the so-called superheavy elements (SHE), generally agreed to be those with atomic numbers larger than 103. These nuclides would be unbound without such effects.

Moreover, it has long been assumed that there ought to exist among the superheavy elements a so-called "island of stability", whereby neutron and proton spherical double-shell closure would lead to enhanced stability and long half-lives, possibly on the order of years [1]. Theoretical evaluations of the stability of as-yet undiscovered nuclides rely in part on neutron- and proton-separation energies. In addition to informing about the location of a superheavy island of stability, the systematic behavior of such quantities would also be useful in determining the maximum extent of bound nuclei.

The atomic masses of isotopes of elements beyond fermium ($Z = 100$), which can presently only be produced online via fusion-evaporation reactions, have until recently been determined only from α decay Q-values along decay chains reaching nuclides with known atomic masses. However, among the transuranium nuclei, such indirect measurements are especially fraught. Among lighter nuclides, the yields are often sufficient to allow precision studies of the nuclear-level structure using modern detectors. For nuclides of superheavy elements, though, it is not uncommon for fewer than some thousands of atoms to have been produced in the entire history of the field. Add to that the fact that

nuclear structure features such as shape deformation [2,3] are prevalent among nuclides of the superheavy elements, leading to numerous isomeric states and complex nuclear level schemes. Especially for lower-yield nuclides, for which sufficiently detailed nuclear spectroscopy to fully determine the nuclear structure is not possible, such indirect mass determinations may suffer systematic errors from, e.g., decay through unknown states.

For nuclei in the so-called "hot fusion island" to the northeast of ^{263}Rf in the nuclear chart, the situation is even more dire. These nuclei, primarily produced in reactions using a ^{48}Ca projectile on an actinide target, have decay chains that uniformly terminate in spontaneous fission prior to reaching well-known nuclides. These nuclides are completely isolated from anything that could be produced in macroscopic quantities. As such, even their identity is confirmed solely from a small set of cross-bombardment studies [4]. As these nuclides would presumably be the as-yet produced species closest to the island of stability, an accurate assessment of the atomic masses within this island would be invaluable – even just one or two anchor-point measurements to provide Q-value connection networks (regardless of concerns about incomplete level schemes) could garner incredible advancements for the nuclear theory of the heaviest elements.

To overcome the problems of compounding errors, which can occur when indirectly determining atomic masses using long decay chains, as well as the lack of mass anchor points in the hot-fusion island, will require the direct determination of atomic masses. However, this is a rather difficult task. As already noted, superheavy elements can only be produced in fusion-evaporation reactions, with the resulting products typically having a few tens of MeV total kinetic energy. Such reaction products are simultaneously too low-energy for the type of magnetic-rigidity and time-of-flight mass determinations, which could be performed at facilities such as SPEG [5], or the S800 [6], while also being too energetic for methods based on ion traps.

In recent years, with improved efficiencies in thermalizing ions using helium gas stopping cells, direct determinations of transuranium nuclides have slowly begun to be possible [7–12]. These measurements are performed by either Penning trap mass spectrometers (PTMS) or multi-reflection time-of-flight mass spectrographs (MRTOF-MS). Herein, we will demonstrate the benefits of the MRTOF-MS technique.

2. Materials and Methods

In the SHE Mass facility, we employ a helium gas cell to thermalize high-energy fusion-evaporation products. A combination of static (DC) and oscillating radio-frequency (RF) electric fields is used to transport the thermalized ions to a small extraction orifice where the combination of electric fields and gas flow whisk the ions into a series of RF ion guides and RF ion traps. In these RF ion traps, ions are prepared for injection into the MRTOF-MS. The MRTOF-MS utilizes specialized ion detectors that incorporate electron multiplication dynodes for detecting the ion impact along with silicon detectors for measuring subsequent nuclear decays. A sketch of the system is given in Figure 1.

The gas cell is installed after the gas-filled recoil ion separator GARIS-II [13], presently located in the E6 vault of the RIKEN Nishina Center for Accelerator-based Science; they were installed in the RILAC hall prior to 2019. A projectile beam with typical energy of $\sim$6 MeV per nucleon impinges a rotating target wheel located just upstream of GARIS-II. With some cross-section, atoms of the projectile will fuse with atoms of the target to form a highly-excited compound nucleus, which will de-excite through particle emission ("evaporation"). Ideally, the particles emitted will be dominantly neutrons (see Section 4) and γ-ray photons. Even for the highest conceivable production cross-sections, the fraction of the projectile beam that undergoes fusion reactions is less than a part per million (ppm) and so the purpose of GARIS-II is to remove the unreacted primary beam while transporting the fusion-evaporation products; see Refs. [13,14] for detailed explanations of how the separation is performed.

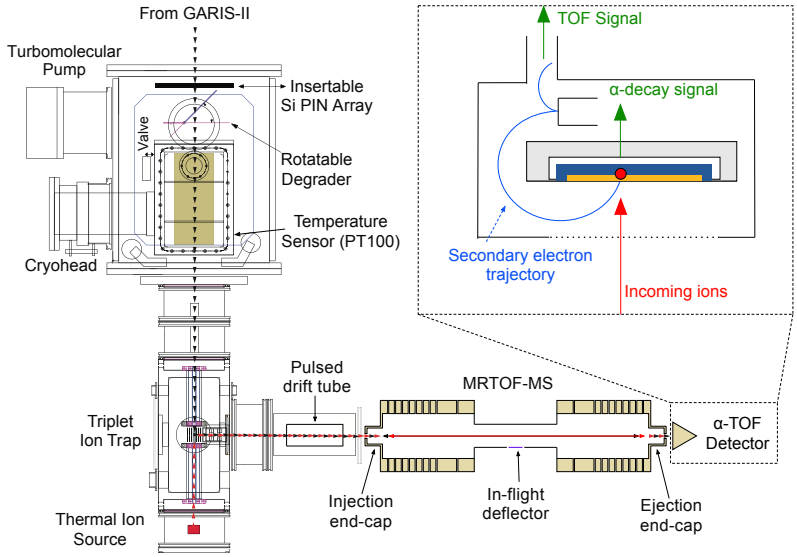

Figure 1. Sketch of the MRTOF-based based SHE-Mass facility located downstream from GARIS-II in the RIKEN Nishina Center. The gas cell has a stopping volume which is 50 cm long. The MRTOF is 1 m long, exclusive of the detector. The inset is a sketch of the alpha-TOF detector which allows decay-correlated mass spectroscopy to be performed by MRTOF-MS.

The gas cell is composed of a re-entrant vacuum chamber, where the outer chamber provides a shield vacuum for the inner chamber. The inner chamber, mounted on a cryohead via an aluminum nitride insulator, houses the stopping volume of the gas cell. The upstream end of the inner chamber is sealed by a 5 μm thick polyimide window reinforced by a 90% transmission aluminum honeycomb mesh. Between the gas cell stopping chamber and GARIS-II is a rotatable energy degrader to reduce the energy of the fusion-evaporation product ions such that they will predominantly stop inside the stopping chamber. When the energy degrader is rotated parallel to the gas cell entrance window, an array of silicon PIN diodes can be inserted to measure the rate of incoming ions when higher yield species are being studied; this allows confirmation of the GARIS-II transport tuning and determination of the overall efficiency of the gas cell and MRTOF system.

The stopping chamber contains a series of annular electrodes to produce a DC drift field. Although prior to 2021, these were composed of a flexible printed circuit board rolled into a tube, they presently comprise an all-metal structure to eliminate charge-up of the polyimide substrate when unstopped energetic particles impinge upon it. At the downstream end of the gas cell is a circular, 10 cm in diameter, traveling wave RF ion carpet [15]. The carpet is printed on a 50 μm polyimide substrate and consists of 80 μm wide annular electrodes separated from one another by 80 μm, mounted to the end of the chamber on an aluminum nitride plate for electrical isolation and thermal wicking. A 250 μm diameter orifice in the center allows ions to exit the gas cell.

The pressure of helium gas in the stopping chamber is regulated to maintain a density equivalent to typically 100 mbar at room temperature; the gas cell is typically cooled to 50 K before online operations in order to freeze out most contaminants. Incoming ions lose energy via ionizing collisions with the helium gas atoms. When the effective thickness of the energy degrader is properly chosen, the incoming ions will lose the last of their kinetic energy via such collisions and come to rest in the gas. The DC field draws the ions toward and presses them to the RF carpet, while an RF pseudopotential—produced by applying signals of opposing RF phases to adjacent electrodes on the RF carpet—repels the ions from the RF carpet. A four-phase audio-frequency (typically 50–100 kHz) traveling wave [16] superimposed on the RF signals draws the ions to the central exit orifice. This process typically requires less than 30 ms.

When the ions reach the central exit orifice, a combination of electric field and gas flow forces them out and into a small (r_0 = 2 mm) RF quadrupole ion guide (QPIG). A DC electric

gradient across the QPIG guides the ions downstream and into a linear Paul trap, which is part of a trio of RF ion traps. This triplet of RF ion traps is composed of a pair of axially segmented linear Paul traps with a special "flat" Paul trap between them [17]. Analyte ions from the gas cell continuously accumulate in one linear Paul trap, while reference ions from a thermal ion source continuously accumulate in the other. They are transferred to the flat trap in an interlaced pattern which we call the "concomitant referencing method" [18]. Every 15 ms, the axial DC electric field in one of the linear Paul traps is modified to transfer its accumulated ions into the flat trap. The ions cool by helium buffer gas ($P \sim 10^{-3}$ mbar) in the flat trap for 3 ms and are then ejected orthogonally via a small hole in the center of the flat trap to be injected into the MRTOF. In this way, the reference and analyte measurements occur essentially simultaneously, and time variations from, e.g., thermal expansion of voltage drifts need not be a source of systematic error.

After ejection from the flat trap, ions pass through a pair of X-Y steering electrodes (not shown in Figure 1), which can be used to correct for slight misalignments between the flat trap and MRTOF and to make the ions enter the MRTOF along its optical axis. The ions then enter a "pulsed drift tube"; changing the bias applied to this element while the ions are inside allows us to adjust the ion energy [19].

The MRTOF consists of a pair of electrostatic ion-optical mirrors separated by a field-free drift region. Both the injection mirror and the ejection mirror are built from 8 annular electrodes, with the outermost "end-cap" electrodes having a cup-shaped attachment to better define the electric field at the entry and exit regions. We presently operate the injection mirror as a "hard mirror" with the five innermost electrodes at the same potential as the central drift tube located between the two mirrors. The ejection mirror uses all eight electrodes to form a "soft mirror" which can produce an energy-isochronous flight path for ions in a specific kinetic energy window. When ions reflect off the energy-isochronous ejection mirror, it slightly counter-rotates the energy-time phase space of the ions. After a certain number of reflections, the phase space will be returned to its initial condition, and the time-of-flight variance among the ions will be minimized, a condition known as the "time focus". A wider annular electrode between the central drift tube and ejection mirror provides spatial focusing for radial confinement. Details of the mechanical design, typical voltage distributions, energy-isochronicity, and time focusing can be found in Refs. [20,21].

Prior to the ejection of ions from the flat trap, the voltage applied to the injection end-cap is reduced by $\Delta V \sim 3$ kV to allow ions to enter the MRTOF. When the ions are near the ejection end-cap, the voltage applied to the injection end-cap is brought high again to trap the ions. Care must be taken in the timing of this voltage transition, as if it occurs while the ions are inside the injection mirror, they will experience a time-varying electric field, which will be a source of systematic error. Ions are allowed to reflect between the two mirrors for a predetermined duration consistent with ions of a given A/q to be in the time-focused condition. At that time, the voltage applied to the ejection end-cap is reduced by $\Delta V \sim 3$ kV to allow ions to leave. The exiting ions implant on the alpha-TOF detector.

The alpha-TOF detector [22,23], shown in the inset image in Figure 1, is a modified MagneTOF detector built in cooperation with ETP Ion Detect, Inc. By inserting a silicon detector into the ion impact plate, this detector allows for detection of the nuclear decay of short-lived radioactive ions subsequent to implantation. The ion time-of-flight is determined by the time between triggering the ejection from the flat trap and the ion impact signal from the alpha-TOF detector, as determined by a time-to-digital converter (MCS6 from FASTCOM Technology).

Prior to an upgrade in 2021, the central drift tube was biased to approximately -1.5 kV, and a constant potential was applied to the pulsed drift tube in Figure 1. This mode required the silicon detector cum ion impact plate to be biased at -2 kV to produce an ion impact signal. This proved to complicate the acquisition of the α-decay signals and to introduce noise that lead to reduced decay energy resolution. As part of the upgrade in 2021, the original self-built high-voltage power supplies [24] were upgraded to EHS Series from ISEG, Inc., and the applied voltages were shifted to allow the central drift tube to be tied to

ground potential. In this configuration, ions require an energy boost via the pulsed drift tube to give them enough energy to enter the MRTOF and later reach the now ground-biased alpha-TOF detector. When the ions flying from the flat trap toward the MRTOF are inside the pulsed drift tube, the potential applied to the pulsed drift tube is increased by a voltage commensurate with the desired ion energy. When the ions leave the drift tube, they accelerate and gain energy equivalent to the change in applied potential. As discussed in Ref [20] this allows very precise control over the ion energy and eases the tuning of the MRTOF-MS voltages.

A further part of the 2021 upgrade to the SHE Mass facility was the installation of an in-flight deflector [20]. This device consists of a set of parallel plates installed at the center of the central drift tube. All but one of the electrodes of the deflector are tied to the ground. By applying small voltage pulses (typically 20 V) to the non-grounded electrode, we can selectively remove ions.

Analysis Methodology

In order to determine atomic masses with the MRTOF-MS, we must first fit the time-of-flight spectral peaks. We have found that our peak shapes tend to be nearly Gaussian, however, they seem to be best represented as exponential-Gaussian hybrid functions defined as

$$f(t) = \begin{cases} \mathrm{A}e^{\delta_\mathrm{L}(2t-2t_c+\delta_\mathrm{L})/2\sigma^2} & \text{if } t \le t_\mathrm{L} \\ \mathrm{A}e^{-(t-t_c)^2/2\sigma^2} & \text{if } t_\mathrm{L} \le t \le t_\mathrm{R} \\ \mathrm{A}e^{\delta_\mathrm{R}(-2t+2t_c+\delta_\mathrm{R})/2\sigma^2} & \text{if } t \ge t_\mathrm{R} \end{cases} \quad (1)$$

where t_c is the peak center, σ^2 is the Gaussian variance, and δ_L (δ_R) is the relative position of the conversion to exponential decay on the left-hand-side (right-hand-side). Figure 2 shows a typical fit obtained in an online measurement prior to the 2021 upgrade, with a mass resolving power of $m/\Delta m \approx 3 \times 10^5$ with a measurement duration of 10 ms.

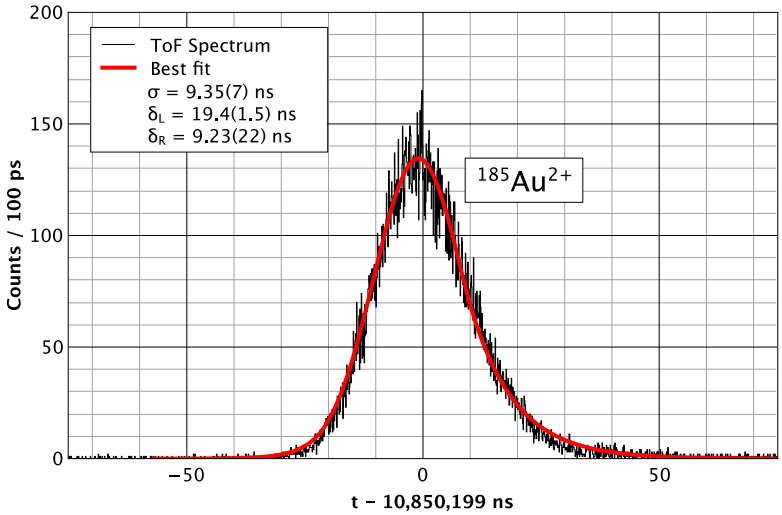

Figure 2. Time-of-flight spectral peak of $^{185}Au^{2+}$ produced online in $^{51}V(^{139}La, p4n)^{185}Au$ reactions. The peak shape can be seen to be well-reproduced by the fitting function. The measurement was performed prior to the recent upgrades, and the mass resolving power is $m/\Delta m = 2.5 \times 10^5$.

In order to determine the atomic mass of our analyte ions, we make use of a single-reference analysis method [17]. In this method, we use a single reference ion species to determine the mass of the analyte as

$$(m/q)_\mathrm{analyte} = (m/q)_\mathrm{ref} \cdot \rho^2 = (m/q)_\mathrm{ref} \left(\frac{t_\mathrm{analyte} - t_0}{t_\mathrm{ref} - t_0} \right)^2 \quad (2)$$

where t_0 is an inherent electronic delay between the start of the TDC clock and the actual ion ejection from the flat trap. The value of this time offset is $t_0 \approx 50$ ns, typically. Before each online measurement, it is calibrated using a pair of well-mass-known analyte species. The contribution of this term falls off quickly with longer times-of-flight, and when the mass-to-charge ratios of analyte and reference are similar, it becomes utterly negligible in the case of an isobaric reference. As the peak shape is nearly Gaussian, the mass precision can be approximated as $\delta m = \frac{m}{\sqrt{N} \cdot \mathrm{MRP}}$ where N is the number of detected ions in the time-of-flight spectrum and MRP is the mass resolving power, $m/\Delta m = 0.5 \cdot t/\Delta t$, where Δx refers to the full-width at half-maximum of variable x. The nearly Gaussian peak shape also allows the performance of ion-by-ion analysis in cases where the yield is too low to perform peak-fitting. In the case of ion-by-ion analysis [12], a mass-to-charge ratio is determined for each analyte ion with an error given by the variance of the high-statistics reference ion spectral peak and the fitting error of the reference peak; in such analysis we only use the reference ions measured ∼5 min before and after the analyte ion to preclude the introduction of any additional statistical or systematic errors from our drift correction algorithm. The atomic mass can then be assigned to the weighted arithmetic mean of the single-ion masses. The error is renormalized to a unity Birge ratio [25] to account for any difference in the mass resolving power achieved for reference and analyte.

In order to analyze very low-yield superheavy nuclides, we make use of a decay-correlated time-of-flight mass spectroscopy method [22,23] to preclude noise or misidentifying a low-yield stable molecular ion for the superheavy nuclide ion. The signals from the silicon detector in the alpha-TOF detector are recorded using a time-stamped multi-channel analyzer aligned with the start of each measurement. For each ion impact signal with a time-of-flight commensurate with the expected flight time of the ion of interest (typically using a ±50 ns wide gate), a search is made for a subsequent alpha-decay with appropriate energy within a correlation time window of typically two half-lives. The detector is only sensitive to decay wherein the alpha-particle is directed toward the silicon detector, and in such a case, the decay daughter will be ejected from the surface, precluding the detection of decay chains. However, in the case when the alpha-particle is directed away from the detector, the decay daughter will be left on the surface, and there is a 50% chance of detecting the daughter decay. In this way, the effective correlation efficiency can be significantly better than 50% by selecting the correlation window to be long enough to include decay daughters and sometimes decay granddaughters. By limiting the mass analysis to ion implantation signals with subsequent decay-correlations, we can confidently work with yields of a few per day or less.

The decay-correlated mass spectroscopy also allows simultaneous determinations of atomic mass and half-life. For each decay correlated to an ion implantation, the implanted atom's lifetime is directly measured. With an ensemble of such measurements, the half-life can be assigned to the arithmetic average of the individual atoms' measured decay times. For measurements of well-studied nuclides, this serves as a useful cross-check on the veracity of the measured atomic mass, while for poorly-studied or newly discovered nuclides, it provides a very efficient spectroscopic analysis.

Moreover, the use of decay-correlated time-of-flight mass spectroscopy allows for an opportunity to resolve low-lying isomeric states that would otherwise be unresolvable with the available mass resolving power of the spectrograph. An example is given in Figure 3 using data published in Ref. [23]. The isomer and ground state of ^{207}Ra requires a mass resolving power of at least 3.5×10^5 to resolve, which exceeded the capability of our MRTOF-MS at the time of the measurement. In Figure 3, an energy gate of two full-widths at half-maximum was made centered on the two known alpha-decay energies, 7320 keV and 7130 keV. The ion implantation signals correlated with the decays within each energy gate were then separated. The time-of-flight center of each oval in Figure 3 is given by the arithmetic average of the times-of-flight of decay-correlated events in each band; the width of each oval is given by two full-widths at half-maximum for the TOF spectrum based on the reference ion peak shape.

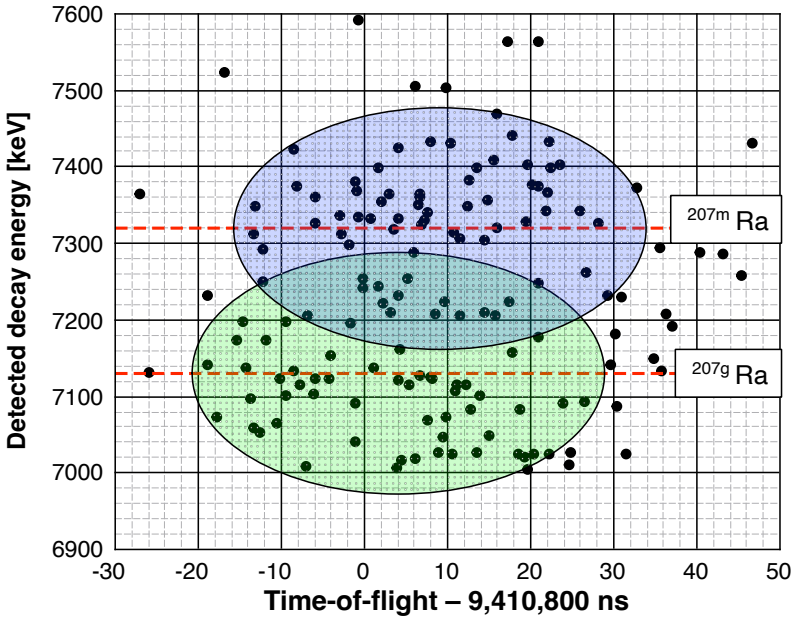

Figure 3. Result of a decay-correlated time-of-flight spectroscopic analysis of ^{207g,m}Ra. The MRTOF-MS did not achieve sufficient mass resolving power to separate the two states, but they could be resolved by including decay energies in the analysis. The blue and green ovals designate ^{207m}Ra and ^{207g}Ra, respectively. The height of the ovals is two full widths at half-maximum of the energy resolution, centered on the known alpha-decay energies of the two states. The width is two full widths at half-maximum of the time-of-flight, centered on the time-of-flight events inside each alpha-decay energy band.

By making two-dimensional ToF-energy fits, it was possible to separately mass analyze the two states ^{207g,m}Ra. Furthermore, it was possible to confirm the state ordering—that is, to confirm that the state with 7320 keV alpha-decays was the isomeric state.

3. Results

The SHE-Mass facility has proven to be highly capable of performing measurements of transuranium and superheavy nuclides. In its first application to such species, in 2017, the isotopes $^{249–252}$Md, produced using a ^{48}Ca beam impinging a ^{205}Tl target, were measured [11]. These nuclides primarily undergo beta-decay, which precludes indirect determinations of their atomic masses. By directly determining their atomic masses, it further allowed the indirect determination of the heavier element nuclides whose alpha-decay chains terminated in these beta-decaying nuclides. At the time of these measurements, neither the alpha-TOF nor the in-flight deflector had yet been implemented. As a result, it was necessary to spend considerable time irradiating a gold target that could not produce the Md isotopes and confirm that no counts were seen under such irradiation. In these early measurements, ^{246}Es and ^{251}Fm were also directly measured for the first time. The six nuclides nearly doubled the number of directly measured transuranium nuclides [7,8].

With the implementation of the alpha-TOF detector, it was possible to tackle low-yield superheavy nuclides. The first candidate was ^{257}Db, which can be produced in the ^{208}Pb(^{51}V, 2n) reaction with a cross-section of ≈2 nb [26]. In an initial measurement, it was possible to determine the mass of ^{257}Db with a relative precision of $\delta m/m \approx 10^{-6}$ [12] based on 11 decay-correlated time-of-flight events across several days.

Of the eleven decay-correlated time-of-flight events in that measurement, seven had decay energies commensurate with ^{257}Db. This nuclide primarily undergoes alpha-decay, emitting alpha-particles with energies near 8875 KeV, 8950 keV, 9050 keV, and 9150 keV. The lower energy alpha-particles have been found to be emitted with a half-life of $T_{1/2}$ = 2.3 s, while the 9150 keV particles are associated with a half-life of $T_{1/2}$ = 0.7 s [27], indicating at least two long-lived states. Unfortunately, the alpha-TOF detector's energy resolution is not

sufficient to unambiguously resolve these various alpha-particles. However, from recent measurements [28], we know the yield ratio for each of these alpha-particles, allowing us to use the known energy resolution of the alpha-TOF detector to then calculate the probability of a decay-correlated time-of-flight event belonging to either the $T_{1/2}$ = 2.3 state or the $T_{1/2}$ = 0.7 state.

We first build a probability function (PDF) for each state based on the detected α-decay signal's energy and the known α-decay energy E_i and relative intensity I_i. Based on the values in Ref. [28], we use

$$P^{T_{1/2}=0.7\ s}(E,\sigma) = 0.39 \cdot e^{-2(E-9155\ \mathrm{keV})^2/\sigma^2} \quad (3)$$

$$P^{T_{1/2}=2.3\ s}(E,\sigma) = \sum_i I_i \cdot e^{-2(E-E_i)^2/\sigma^2}, \quad (4)$$

where E is the detected α-decay energy, σ is the energy resolution of the alpha-TOF detector, and the set of (I_i, E_i) is (0.02, 8856 keV), (0.35, 8965 keV), and (0.24, 9066 keV). Using this, we can use a set of decay-correlated time-of-flight mass spectroscopy data to estimate which of the two states is the ground state and which is the isomer. To do so, we first separately re-weight the mass uncertainty of each data point as

$$\delta m' = \delta m / P^j(E_\alpha) \quad (5)$$

for each state j, where j represents the two states of ^{257}Db ($T_{1/2}$ = 0.7 s and $T_{1/2}$ = 2.3 s) in this case. Next, we calculate the weighted average mass for both states from the data set. If either the energy resolution or mass resolving power were sufficient to fully resolve the states, we could expect to unambiguously ascertain the excitation energy and state order from such an evaluation. However, since neither detector presently meets such conditions, we must estimate our confidence in such an evaluation based on simulations.

To this end, we made a fairly simple Monte Carlo (MC) simulation (see Supplementary Materials) to estimate the effect. From the MC simulations, we determined that without the ability to either resolve the two states in time-of-flight or to fully resolve the α-decay energies, the evaluation tended, on average, to underestimate the excitation energy. However, the MC calculations also confirmed that the state ordering could be reasonably well determined even with few decay-correlated events, as shown in Figure 4.

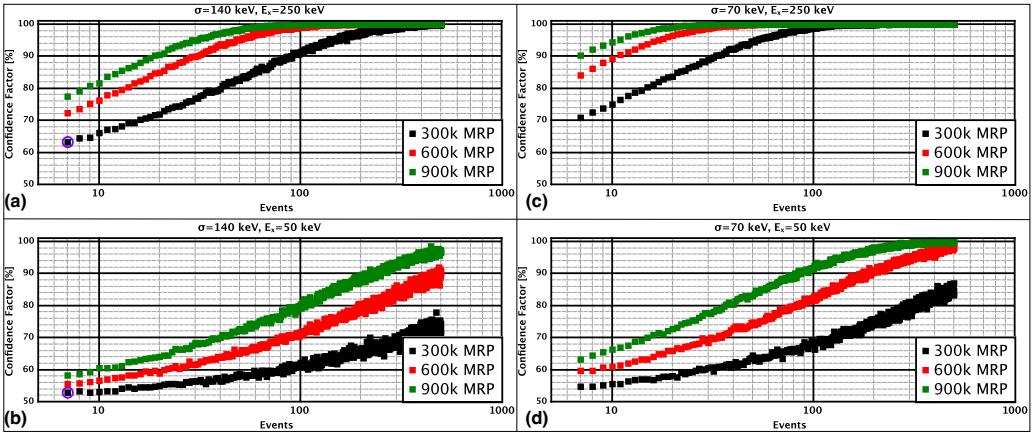

Figure 4. Results of Monte Carlo simulations to estimate the confidence with which we can determine the state ordering using a small number of decay-correlated time-of-flight events for ^{257}Db assuming (**a**) isomeric excitation and α-decay energy resolution of (**a**) 250 keV and 140 keV, (**b**) 50 keV and 140 keV, (**c**) 250 keV and 70 keV, (**d**) 50 keV and 70 keV. The blue circles are indicative of the previously published data set.

Figure 5 shows the atomic mass assigned to each of the seven time-of-flight events relative to the 2020 Atomic Mass Evaluation (AME2020) [29] value for the mass of ^{257g}Db,

as a function of the measured energy of the alpha-decay subsequent to ion implantation. For reference, the figure also includes the PDF for each state of ^{257}Db. For each event, we re-weight the atomic mass error according to Equation (5) based on the detected alpha-decay energy. When we use our previously published data set to calculate the weighted average atomic mass for the $T_{1/2}$ = 1.8 s state, we find it differs from the AME2020 value by Δm = 23(260) keV/c^2. For the $T_{1/2}$ = 0.7 s state, the weighted average differs from AME2020 value by Δm = −344(260) keV/c^2. This would imply the $T_{1/2}$ = 0.7 s state would be the ground state. Based on our Monte Carlo simulations and a presumption that the isomeric excitation is energy is more than 50 keV but less than 350 keV, we can offer this assessment with between 53% and 67% confidence based on the 7 events observed in our first run.

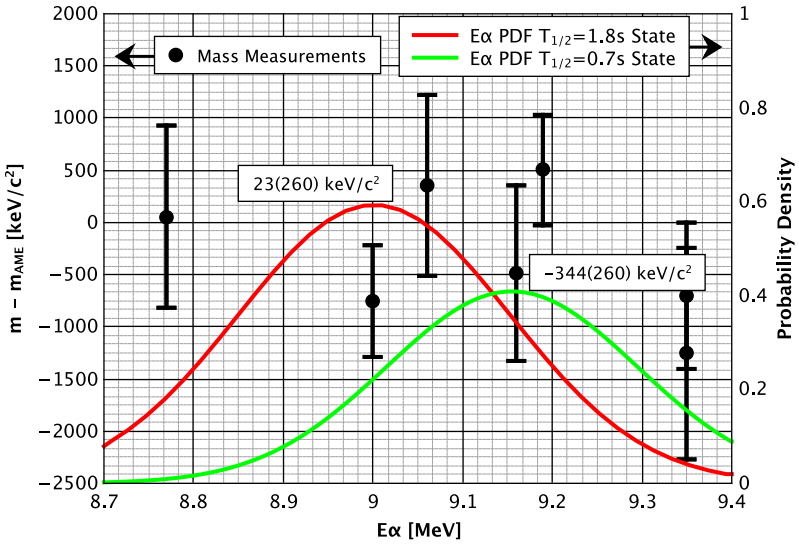

Figure 5. Atomic mass determined for each of seven decay-correlated time-of-flight events commensurate with alpha-decay of ^{257}Db, a function of detected alpha-decay energy. The probability density functions (PDF) for the longer- and shorter-lived states of ^{257}Db are also shown in red and green, respectively. By including a weight from each PDF in evaluating the weighted average, we can estimate the state ordering and excitation energy.

4. Summary and Outlook

After our initial measurement of the atomic mass of ^{257}Db, we have made significant improvements. The energy resolution of the alpha-TOF has been improved from σ = 150 keV to σ = 75 keV. The typical mass resolving power has been improved from $m/\Delta m = 2.5 \times 10^5$ to $m/\Delta m = 8{\times}10^5$. The system efficiency for ions delivered by GARIS-II to reach the alpha-TOF detector after ∼700 reflections in the MRTOF is now 5–10%. The addition of the in-flight deflector now allows much higher confidence in the A/q identification of all time-of-flight spectral peaks by limiting the circulating ions to those of a desired set of A/q values. With the improved performance, an ensemble of ten decay-correlated time-of-flight events commensurate with the decay of ^{257}Db would allow at least 85% confidence in the determination of the state ordering presuming an excitation energy of at least 100 keV.

With these improvements, another measurement was recently made for ^{257,258}Db with ≈20 decay-correlated time-of-flight events detected for each nuclide. The analysis is ongoing, but a preliminary comparison to previously published results is provided for ^{257}Db in Figure 6. In a near-future measurement, we will seek to measure ^{255,256}Db as well, which will allow a meaningful discussion of nuclear structure around N = 152. Accelerator time has also been approved for producing ^{259}Sg via the ^{209}Bi(^{51}V, 1n) reaction for MRTOF-based decay-correlated mass spectroscopy.

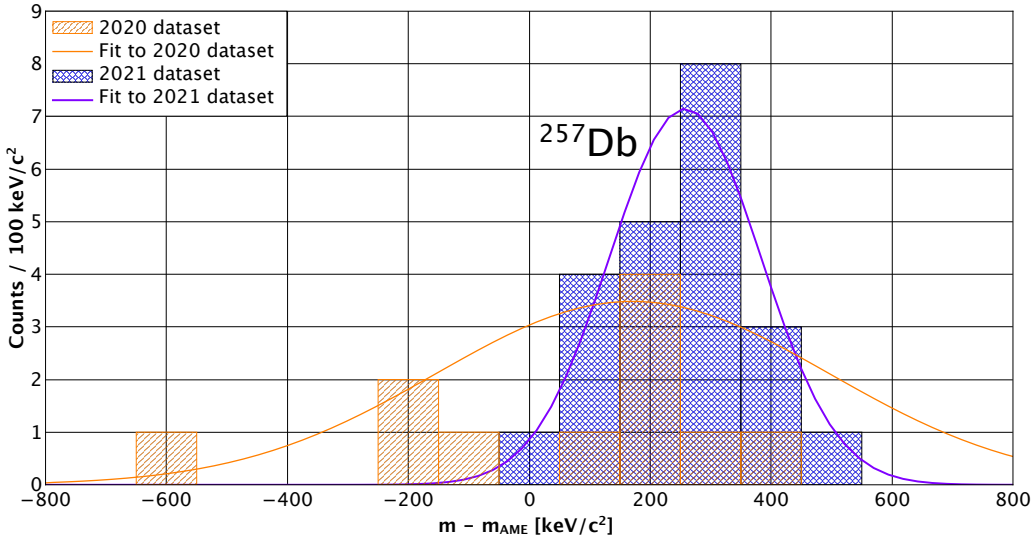

Figure 6. Comparison of previously published [12] ("2020 dataset") results for ^{257}Db with a preliminary analysis of data taken after upgrading the SHE-Mass facility. The detection rate and mass resolution can be seen to have clearly improved. Fits are based on the mass resolution of simultaneously obtained reference ion spectra. The MRTOF achieved a mass resolving power of 3×10^5 in the first measurements and 8×10^5 after the upgrades.

Of more value, perhaps, is the approved measurement of Mc and Nh isotopes. The nuclides ^{287,288}Mc and their decay daughters ^{283,284}Nh are located on the isolated "hot fusion island" where all nuclides' decay chains terminate in spontaneous fission. Due in part to this isolation, the Provisional Report of the 2017 Joint Working Group of IUPAC and IUPAP [30] recommended the development of orthogonal means to confirm A and Z of nuclides in this region and offered the suggestion that sufficiently precise atomic mass measurements might be one possible means of such. With our MRTOF-based decay-correlated mass spectroscopy technique, this would be quite possible to achieve.

Using the reaction ^{243}Am(^{48}Ca,xn), we expect the yield of ^{287,288}Mc should be sufficient to produce a few decay-correlated time-of-flight events per week. A fraction of the ^{287,288}Mc will decay to ^{283,284}Nh in the gas cell, providing at least one decay-correlated time-of-flight event per week. With a single decay-correlated time-of-flight event, we could confirm the atomic mass number A with absolute certainty. With the present mass resolving power of $m/\Delta m = 8 \times 10^5$, it would only require four decay-correlated time-of-flight events to determine the atomic mass to a precision of $\delta m \approx 150$ keV/c^2. With such precision, a comparison to theoretical atomic mass predictions can be made; across a great variety of models, there are unambiguous gaps between Z values across the isobaric chains in this region. By comparing a directly determined atomic mass of precision $\delta m < 200$ keV/c^2 to theoretical models, it should be possible to provide an orthogonal determination of Z with high confidence. Forty days of accelerator time has been approved for such a measurement and will be run as soon as a supply of ^{48}Ca can be procured.

In summary, the multi-reflection time-of-flight mass spectrograph has proven to be of great utility in analyzing superheavy nuclides. The use of decay-correlated time-of-flight mass spectroscopy allows very high confidence in the identification of even extremely low-yield superheavy nuclides. The current performance characteristics of the MRTOF and alpha-TOF at the SHE-Mass facility are sufficient to determine, with reasonable confidence, the state ordering in superheavy nuclides that exhibit multiple long-lived states. Future improvements in alpha-TOF energy resolution should allow yet higher confidence in state ordering and hopefully will reach the level where excitation energy can be determined for even low-lying states by fully resolving the α-decay spectrum.

Figure 7 shows the present state of direct mass determinations among transfermium nuclides. Several isotopes of No and Lr, and one isotope of Rf, have been measured by

Penning trap mass spectroscopy [8–10]. Four isotopes of Md and one isotope of No were measured [11] by MRTOF-MS prior to the development of the decay-correlated time-of-flight mass spectroscopy technique, while two isotopes of Db have been measured [12,31,32] using decay-correlated time-of-flight mass spectroscopy. In the near future, we plan to use decay-correlated mass spectroscopy to measure the mass of ^{256}Db and search for ^{255}Db, as well as to measure the mass of ^{259}Sg. When the Nishina Center for Accelerator-based Science can again supply a ^{48}Ca projectile beam, we will use the technique to unambiguously determine A and Z for neutron-rich Mc and Nh isotopes and provide mass anchor points for the isolated nuclides in the "hot-fusion island".

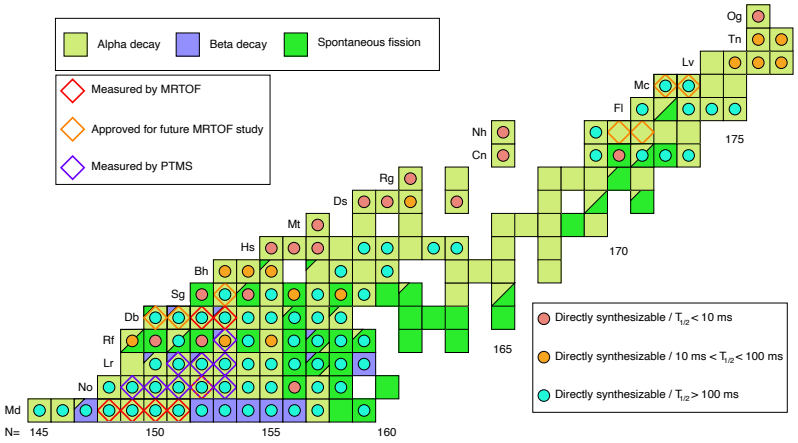

Figure 7. Table of known transfermium nuclides. The nuclides with half-lives longer than 10 ms would be candidates for MRTOF-based decay-correlated time-of-flight mass spectroscopy.

Supplementary Materials: The following supporting information can be downloaded at: https://www.mdpi.com/article/10.3390/atoms11100134/s1, File SO.cpp: Computer code (C++) used in the Monte Carlo calculation presented in Figure 4.

Author Contributions: All authors have contributed significantly to this work. All authors contributed to conceptualization and methodology; software: P.S. and M.W.; funding acquisition: M.W.; writing–original draft preparation: P.S. All authors have read and agreed to the published version of the manuscript.

Funding: This work was supported by the Japan Society for the Promotion of Science KAKENHI (Grants Nos. 20740165, 24224008, 24740142, 15H02096, 15K05116, 17H06090, 18H03711, 19K03899, 22H04946, and 23K13132).

Institutional Review Board Statement: "Not applicable" as these studies did involve human or animal subjects.

Data Availability Statement: The authors will consider sharing of data sets, computer code, and mechanical drawings when directly contacted via email by interested parties.

Acknowledgments: We wish to express gratitude to the Nishina Center for Accelerator-Based Science at RIKEN and the Center for Nuclear Study at the University of Tokyo for their support of online measurements

Conflicts of Interest: The authors declare no conflict of interest. The funders had no role in the design of the study, in the collection, analyses, or interpretation of data, in the writing of the manuscript, or in the decision to publish the results.

Abbreviations

The following abbreviations are used in this manuscript:

RF	Radiofrequency
MRTOF	Multi-reflection time-of-flight (mass spectrograph)
MRTOF-MS	Multi-reflection time-of-flight mass spectrograph
TOF	Time-of-flight

References

1. Fiset, E.O.; Nix, J.R. Calculation of half-lives for superheavy nuclei. *Nucl. Phys. A* **1972**, *193*, 647–671. [CrossRef]
2. Herzberg, R.D.; Greenless, P.T. In-beam and decay spectroscopy of transfermium nuclei. *Prog. Part. Nucl. Phys.* **2008**, *61*, 674. [CrossRef]
3. Heenen, P.-H.; Skalski, J.; Staszczak, A.; Vretenar, D. Shapes and α-and β-decays of superheavy nuclei. *Nucl. Phys. A* **2015**, *944*, 415–441. [CrossRef]
4. Forsberg, U.; Rudolph, D.; Fahlander, C.; Golubev, P.; Sarmiento, L.G.; Åberg, S.; Block, M.; Düllmann, C.E.; Heßberger, F.P.; Kratz, J.V.; et al. A new assessment of the alleged link between element 115 and element 117 decay chains. *Phys. Lett. B* **2016**, *760*, 293–296. [CrossRef]
5. Lima, G.F.; Lepine-Szily, A.; Audi, G.; Mittig, W.; Chartier, M.; Orr, N.A.; Lichtenthaler, R.; Angelique, J.C.; Casandjian, J.M.; Cunsolo, A.; et al. Direct mass measurements of proton-rich isotopes of Ge, As, Se, and Br. *Phys. Rev. C* **2002**, *65*, 044618. [CrossRef]
6. Bazin, D.; Caggiano, J.; Sherrill, B.; Yurkon, J.; Zeller, A. The S800 spectrograph. *Zeller Nucl. Instrum. Methods Phys. Res. B* **2003**, *204*, 629–633. [CrossRef]
7. Eibach, M.; Beyer, T.; Blaum, K.; Block, M.; Dullmann, C.E.; Eberhardt, K.; Grund, J.; Nagy, S.; Nitsche, H.; Nortershauser, W.; et al. Direct high-precision mass measurements on ^{241,243}Am, ^{244}Pu, and ^{249}Cf. *Phys. Rev. C* **2014**, *89*, 064318. [CrossRef]
8. Dworschak, M.; Block, M.; Ackermann, D.; Audi, G.; Blaum, K.; Droese, C.; Eliseev, S.; Fleckenstein, T.; Haettner, E.; Herfurth, F.; et al. Penning trap mass measurements on nobelium isotopes. *Phys. Rev. C* **2010**, *81*, 064312. [CrossRef]
9. Ramirez, E.M.; Ackermann, D.; Blaum, K.; Block, M.; Droese, C.; Düllmann, C.E.; Dworschak, M.; Eibach, M.; Eliseev, S.; Haettner, E.; et al. Direct mapping of nuclear shell effects in the heaviest elements. *Science* **2012**, *337*, 1207. [CrossRef]
10. Kaleja, O.; Anđelić, B.; Bezrodnova, O.; Blaum, K.; Block, M.; Chenmarev, S.; Chhetri, P.; Droese, C.; DüllmannandCh, E.; Eibach, M.; et al. Direct high-precision mass spectrometry of superheavy elements with SHIPTRAP. *Phys. Rev. C* **2022**, *106*, 054325. [CrossRef]
11. Ito, Y.; Schury, P.; Wada, M.; Arai, F.; Haba, H.; Hirayama, Y.; Ishizawa, S.; Kaji, D.; Kimura, S.; Koura, H.; et al. First Direct Mass Measurements of Nuclides around Z = 100 with a Multireflection Time-of-Flight Mass Spectrograph. *Phys. Rev. Lett.* **2018**, *120*, 152501. [CrossRef] [PubMed]
12. Schury, P.; Niwase, T.; Wada, M.; Brionnet, P.; Chen, S.; Hashimoto, T.; Haba, H.; Hirayama, Y.; Hou, D.S.; Iimura, S.; et al. First high-precision direct determination of the atomic mass of a superheavy nuclide. *Phys. Rev. C* **2021**, *104*, L021304. [CrossRef]
13. Kaji, D.; Morimoto, K.; Sato, N.; Yoneda, A.; Morita, K. Gas-filled recoil ion separator GARIS-II. *Nucl. Instrum. Methods Phys. Res. Sect. B* **2013**, *317*, 311–314. [CrossRef]
14. Kimura, S.; Kaji, D.; Ito, Y.; Miyatake, H.; Morimoto, K.; Schury, P.; Wada, M. Reduction of contaminants originating from primary beam by improving the beam stoppers in GARIS-II. *Nucl. Instrum. Method Phys. Res. A* **2021**, *992*, 164996. [CrossRef]
15. Arai, F.; Ito, Y.; Wada, M.; Schury, P.; Sonoda, T.; Mita, H. Investigation of the ion surfing transport method with a circular rf carpet. *Int. J. Mass Spectrom.* **2014**, *362*, 56–58. [CrossRef]
16. Bollen, G. "Ion surfing" with radiofrequency carpets. *Int. J. Mass Spectrom.* **2011**, *299*, 131–138. [CrossRef]
17. Ito, Y.; Schury, P.; Wada, M.; Naimi, S.; Smorra, C.; Sonoda, T.; Mita, H.; Takamine, A.; Okada, K.; Ozawa, A.; et al. A novel ion cooling trap for multi-reflection time-of-flight mass spectrograph. *Nucl. Instrum. Methods Phys. Res. Sect. B* **2013**, *317*, 544–549. [CrossRef]
18. Schury, P.; Ito, Y.; Rosenbusch, M.; Miyatake, H.; Wada, M.; Wollnik, H. Improving wide-band mass measurements in a multi-reflection time-of-flight mass spectrograph by usage of a concomitant measurement scheme. *Int. J. Mass Spectrom.* **2018**, *433*, 40–46. [CrossRef]
19. Rosenbusch, M.; Wada, M.; Chen, S.; Takamine, A.; Iimura, S.; Hou, D.; Xian, W.; Yan, S.; Schury, P.; Hirayama, Y.; et al. The new MRTOF mass spectrograph following the ZeroDegree spectrometer at RIKEN's RIBF facility. *Nucl. Instrum. Methods Phys. Res. Sect. A* **2023**, *1047*, 167824. [CrossRef]
20. Rosenbusch, M.; Ito, Y.; Schury, P.; Wada, M.; Kaji, D.; Morimoto, K.; Haba, H.; Kimura, S.; Koura, H.; MacCormick, M.; et al. New mass anchor points for neutron-deficient heavy nuclei from direct mass measurements of radium and actinium isotopes. *Phys. Rev. C* **2018**, *97*, 064306. [CrossRef]
21. Schury, P.; Wada, M.; Ito, Y.; Arai, F.; Naimi, S.; Sonoda, T.; Wollnik, H.; Shchepunov, V.A.; Smorra, C.; Yuan, C. A high-resolution multi-reflection time-of-flight mass spectrograph for precision mass measurements at RIKEN/SLOWRI. *Nucl. Instrum. Methods Phys. Res. Sect. B Beam Interact. Mater. Atoms* **2014**, *335*, 39. [CrossRef]
22. Niwase, T.; Wada, M.; Schury, P.; Haba, H.; Ishizawa, S.; Ito, Y.; Kaji, D.; Kimura, S.; Miyatake, H.; Morimoto, K.; et al. Development of an "α-TOF" detector for correlated measurement of atomic masses and decay properties. *Nucl. Instrum. Methods Phys. Res. Sect. Accel. Spectrometers Detect. Assoc. Equip.* **2020**, *953*, 163198. [CrossRef]
23. Niwase, T.; Wada, M.; Schury, P.; Brionnet, P.; Chen, S.D.; Hashimoto, T.; Haba, H.; Hirayama, Y.; Hou, D.S.; Iimura, S.; et al. α-decay-correlated mass measurement of ^{206,207g,m}Ra using an α-TOF detector equipped multireflection time-of-flight mass spectrograph system. *Phys. Rev. C* **2021**, *104*, 044617. [CrossRef]
24. Wada, M.; Schury, P. Stable high-voltage supplies for MRTOF mass spectrograph. *RIKEN Accel. Prog. Rep.* **2011**, *44*, 163.
25. Birge, R.T. The calculation of errors by the method of least squares. *Phys. Rev.* **1932**, *40*, 207. [CrossRef]

26. Gates, J.M.; Nelson, S.L.; Gregorich, K.E.; Dragojević, I.; Düllmann, C.E.; Ellison, P.A.; Folden, C.M., III; Garcia, M.A.; Stavsetra, L.; Sudowe, R.; et al. Comparison of reactions for the production of ^{258,257}Db:^{208}Pb(^{51}V,*xn*) and ^{209}Bi(^{50}Ti,*xn*). *Phys. Rev. C* **2008**, *78*, 034604. [CrossRef]
27. Heßberger, F.P.; Antalic, S.; Ackermann, D.; Heinz, S.; Hofmann, S.; Khuyagbaatar, J.; Kindler, B.; Kojouharov, I.; Lommel, B.; Mann, R. Alpha-decay properties of ^{261}Bh. *Eur. Phys. J. A* **2010**, *43*, 175–180. [CrossRef]
28. Brionnet, P. Etude Des États Isoméres des Noyaux Superlourds: Cas des Noyaux. Ph.D. Thesis, Universitè de Strasbourg, Strasbourg, France , 2017.
29. Wang, M.; Huang, W.J.; Kondev, F.G.; Audi, G.; Naimi, S. The AME 2020 atomic mass evaluation (II). Tables, graphs and references. *Chin. Phys. C* **2021**, *45*, 030003. [CrossRef]
30. Hofmann, S.; Dmitriev, S.N.; Fahlander, C.; Gates, J.M.; Roberto, J.B.; Sakai, H. On the discovery of new elements (IUPAC/IUPAP Provisional Report) Provisional Report of the 2017 Joint Working Group of IUPAC and IUPAP. *Pure Appl. Chem.* **2018**, *90*, 1774. [CrossRef]
31. Schury, P.; Niwase, T.; Wada, M.; Brionnet, P.; Chen, S.; Hashimoto, T.; Haba, H.; Hirayama, Y.; Hou, D.S.; Iimura, S.; et al. Improved mass measurement of 257Db by decay-correlated mass spectroscopy. *RIKEN Accel. Prog. Rep.* **2022**, *55*, 6.
32. Schury, P.; Niwase, T.; Wada, M.; Brionnet, P.; Chen, S.; Hashimoto, T.; Haba, H.; Hirayama, Y.; Hou, D.S.; Iimura, S.; et al. Initial mass measurement of 258Db by decay-correlated mass spectroscopy. *RIKEN Accel. Prog. Rep.* **2022**, *55*, 7.